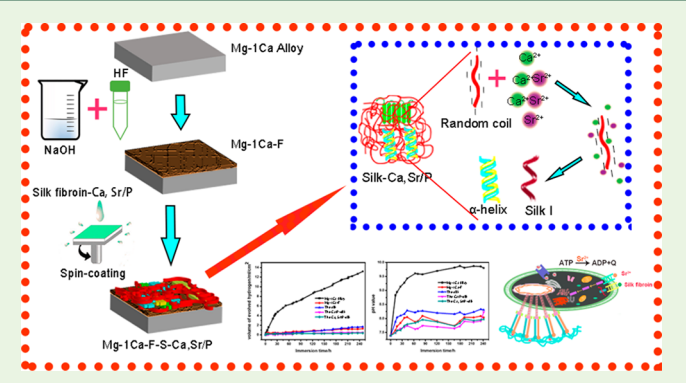


Biomimetic Ca, Sr/P-Doped Silk Fibroin Films on Mg-1Ca Alloy with **Dramatic Corrosion Resistance and Osteogenic Activities**

Pan Xiong,[†] Zhaojun Jia,[†] Ming Li,[‡] Wenhao Zhou,[†] JiangLong Yan,[†] Yuanhao Wu,[†] Yan Cheng,*,[†] and Yufeng Zheng*, \$6

ABSTRACT: Magnesium and its alloys have emerged as some of the most promising biodegradable metals for temporary bone implants, but challenges remain in controlling their corrosion and biocompatibility and endowing them with bioactivity and osteogenic functionality. Herein, we presented newly developed bioactive Ca, Sr/P-containing silk fibroin films (the Ca, Sr/P silk) on top of Mg-1Ca alloy to simultaneously improve the corrosion resistance, osteocompatibility, and osteogenic activities important in maintaining mechanical integrity and stimulating bone formation, respectively. Briefly, extracellular matrix (ECM) mimicking Ca, Sr/P silk fibroin films were constructed layer upon layer on fluoridized Mg-1Ca alloy via simple spinning assembly.



The corrosion resistance property of different samples was studied in vitro by immersion experiments and electrochemistry measurements in Hanks' solution, with the silk-coated ones showing over 1 order of magnitude increase in corrosion resistance compared to the uncoated. Particularly, the Ca, Sr/P silk had the best anticorrosion performance, presumably because of better retaining of the β -sheet silk conformation and ion-induced structural conversion from random coils to silk I and α -helices. Furthermore, the preliminary study of the corrosion behavior of the Ca, Sr/P silk was confirmed the availability of the films for corrosion resistance improvement. The osteocompatibility and osteogenic activities were evaluated by the multiple osteoblast (MC3T3-E1) responses, i.e., proliferation, adherence, spreading, and differentiation in vitro. The Ca, Sr/P silk exhibited the optimal osteogenic activity among all experimental groups. These preliminary results comprehensively confirmed the validity of the coating strategy and they implicated the great potential of the modified Mg alloys as degradable bone implants.

KEYWORDS: biomedical Mg alloy, surface modification, silk fibroin films, Ca, Sr/P, degradation, corrosion resistance, biocompatibility, osteogenesis

1. INTRODUCTION

With unique physicochemical properties, biodegradability, and biocompatibility, magnesium and its alloys have drawn increasing research attention, especially in the field of cardiovascular and orthopedic biomaterials. 1-7 It is suggested that as biodegradable bone implant materials, magnesium and its alloys should maintain their mechanical integrity over a period of 12-18 weeks to allow bone healing. 1,8 However, the overwhelmingly high corrosion rate in body fluids in contrast to the tissue healing rate can lead to rapid deterioration of the mechanical integrity, greatly limiting their clinical application.⁹ In addition, heavy corrosion results in local alkalosis and continuing release of copious hydrogen that would separate implants from host tissue layers. 6,8 Mg-1Ca alloy is one of the newly designed promising magnesium alloys. It displays excellent mechanical property and beneficial effects on bone healing with coreleased Mg and Ca ions, but poor corrosion resistance.8 Thus, improving the corrosion resistance of Mg-

1Ca alloy is urgent and of foremost importance. To this end, a number of surface modification methods have been developed, 10,11 among which fluoride treatment 12-14 and polymeric coatings 15-17 are most common. However, the fluoride-treated surfaces tend to possess undesired cracks, thus needing further handling. 18 Despite their potential to load functional drugs and biomolecules, polymeric coatings are generally porous, and the biosafety of both the polymers and their degradation products is still under debate.

Silk fibroin is a natural protein extracted from Bombyx mori silkworms,²⁰ which has excellent mechanical properties,²¹ good biocompatibility,²² absent immunogenicity,²² limited bacterial adhesion,²³ and controllable biodegradability.^{22–24} It owns the unique characteristic with the variable second structures

Received: July 11, 2018 Accepted: August 13, 2018 Published: August 13, 2018

[†]Academy for Advanced Interdisciplinary Studies, Peking University, Beijing 100871, China

[‡]China-America Institute of Neuroscience, Xuanwu Hospital, Capital Medical University, Beijing, 100053, China

[§]Department of Materials Science and Engineering, College of Engineering, Peking University, Beijing 100871, China

including random coils, α -helices, β -sheets, and β -turns. The transition among the second structure is thought to be largely brought by extensional shearing, although variations in pH, metallic ion contents, and water content are thought to make a contribution as well. Silk fibroin films have been researched for many years, in comparison to other polymeric films researched in biomedical materials, and they show better mechanical property than collagen and slighter foreign body response than the synthetic polymers poly(3-hydroxybutyrate) (PHB), poly(caprolactone), polyamide, and PLA. Notably, the particular second structure of silk fibroin endows the films with tunable mechanical properties, biocompatibility, and biodegradation rate. The second structure of silk fibroin endows the films with tunable mechanical properties, biocompatibility, and biodegradation rate.

As we know, natural bone is a composite of mineral phase (mainly the apatite) and an organic matrix.²⁸ Thus, the fabrication of inorganic-organic hybrid films on bone implants sounds appealing. Especially, silk fibroin has an intrinsic resemblance to the arranged collagen in bone matrix that builds a 3D framework where minerals are deposited.²⁹ Through biomimetic mineralization,³⁰ mechanochemical route^{31°} or coprecipitation methods,³² silk fibroin can be easily complexed with calcium phosphates to form organic/inorganic hybrids, which have excellent mechanical properties and osteogenesis activity^{33,34} and improved biocompatibility and bioactivity. 35,36 On the other hand, strontium is one of the trace elements in natural bone. It is confirmed that Sr addition into calcium phosphate biomaterials is shown to facilitate the attachment and proliferation of osteo-precursor cells. 37,38 Ke Yang et al. found that coating Mg-Sr alloy with a Sr-Ca-Pcontaining MAO film encouraged new bone formation in vivo.³⁹ Up to now, strontium-doped Ca/P silk fibroin materials have been rarely reported regardless of the numerous studies on Ca/P silk fibroin films.

In this work, we are the first to demonstrate a bioactive ECM-like films on Mg-1Ca alloy by facile spinning assembly of Ca, Sr/P inorganic salts/silk fibroin hybrids, as generated from in situ coprecipitation, aiming to improve the corrosion resistance and surface bioactivity and osteogenic capacity of the substrate. The fabrication process is illustrated in Figure 1. The fluoride treatment served as a pretreatment, which was generally used to improve film/substrate adhesion and allow for further functionalization. The Notably, the addition of Ca, Sr/P components into silk fibroin can aid in maintaining appropriate conformation of β -sheets and reducing the number

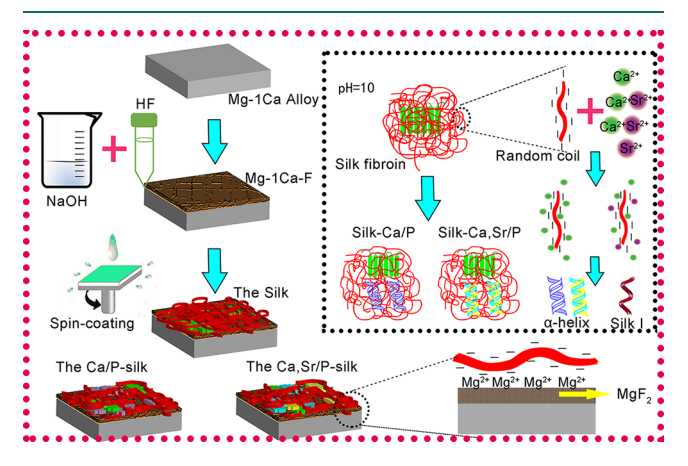


Figure 1. Schematic of the films fabrication process, the inset is the interaction between the metal ions (Ca^{2+}, Sr^{2+}) and silk fibroin.

of random coils, which in return might enhance the corrosion resistance and improve the biocompatibility and bioactivity of the surface. This work presents a new simple and efficient method for the surface modification of biodegradable magnesium alloys and it provides some new insights into the physicochemical and biological properties of silk fibroin protein materials for biomedical applications.

2. MATERIALS AND METHODS

The preparation of extruded Mg-1Ca(wt %) alloy samples is detailed in our previous work. ¹⁸ The chemicals, including NaOH, HF, $Ca(NO_3)_2$, $Sr(NO_3)_2$, and K_2HPO_4 were purchased from Beijing Chemical Reagent Co., Ltd., China. All other reagents, unless otherwise specified, are of reagent grade.

- **2.1. Specimens Preparation.** The extruded Mg-1Ca (wt %) alloy with a diameter of 12 mm was cut into 2 mm thick slices and then ground by SiC paper up to 2000 grit; subsequently dipped into acetone, ethanol, and deionized water with ultrasonic washer for 10 min respectively; and then dried by cold-air blowing.
- **2.2. Fluoride Pretreatment.** A two-step method was used to complete the fluoride pretreatment. The basic reaction is as follows:

$$Mg + 2OH^{-} = Mg(OH)_{2}$$
 (1)

$$Mg(OH)_2 + 2HF = MgF_2 + 2H_2O$$
 (2)

At the first step, all samples were immersed in the boiling NaOH solution (200 g/L) for 3 h, the volume of NaOH solution was related to the number of samples with the rate of 10 mL/cm 2 . To react uniformly, the solution was stirred. After the reaction completed, samples were rinsed with deionized water three times and dried with cold air.

Ten milliliter plastic centrifuge tubes were filled with 9 mL of HF. Each specimen was immersed into one centrifuge tube. The tubes were then incubated in an oven at 60 $^{\circ}\text{C}$ for 6 h. Finally, all samples were dried at room temperature.

2.3. Preparation of Silk Fibroin Films. Silk fibroin solution was extracted as the previous study. ⁴⁰ *Bombyx mori.* cocoons were cut into pieces and boiled in 2 L of 0.02 M Na₂CO₃ solution for 30 min to remove the sericin fibroin, which was reported to cause the inflammatory. ⁴¹ The degummed silk was rinsed with deionized water for three times and dried in air overnight. The dried silk fibroin was solubilized in 9.3 M LiBr solution at 60 °C for 4 h and dialyzed against water for 3 days. The final concentration of silk fibroin solution was 8 w/v%.

The silk fibroin solution was diluted to 2 w/v%. A certain amount of $Ca(NO_3)_2$ (0.1 mol/L), $Sr(NO_3)_2$ (0.1 mol/L), and K_2HPO_4 (0.1 mol/L) were added into the silk fibroin solution, and all the solutions were buffered to pH 10 with 1 mol/L NaOH. The composition of solutions used for films were listed in Table 1. To get better mechanical properties, PEG_{200} was also added into the solution, according to the previous work.

A Model KW-4A spin coater (Si-you-yen, Beijing, China) was employed with a low rotation speed of 1500 rpm for 15 s as well as a high rotation speed of 3500 rpm for 10 s at room temperature. 50 μ L of each silk fibroin solution as above was added to the specimen for a cycle, and there were 5 repeated times for each side of the samples. All

Table 1. Composition of the Solutions Used for Films

| films | 2% silk fibroin (mL) | 0.1 mol/L Ca(NO ₃) ₂ (mL) | 0.1 mol/L Sr(NO ₃) ₂ (mL) | $\begin{array}{c} 0.1 \text{ mol/L} \\ \text{K}_2 \text{HPO}_4 \\ \text{(mL)} \end{array}$ | PEG ₂₀₀ (mL) |
|---------------------|----------------------------|--|--|--|-------------------------|
| silk | 5 | 0 | 0 | 0 | 0.1 |
| Ca/P silk | 5 | 1 | 0 | 0.6 | 0.1 |
| Ca, Sr/P silk | 5 | 0.9 | 0.1 | 0.6 | 0.1 |

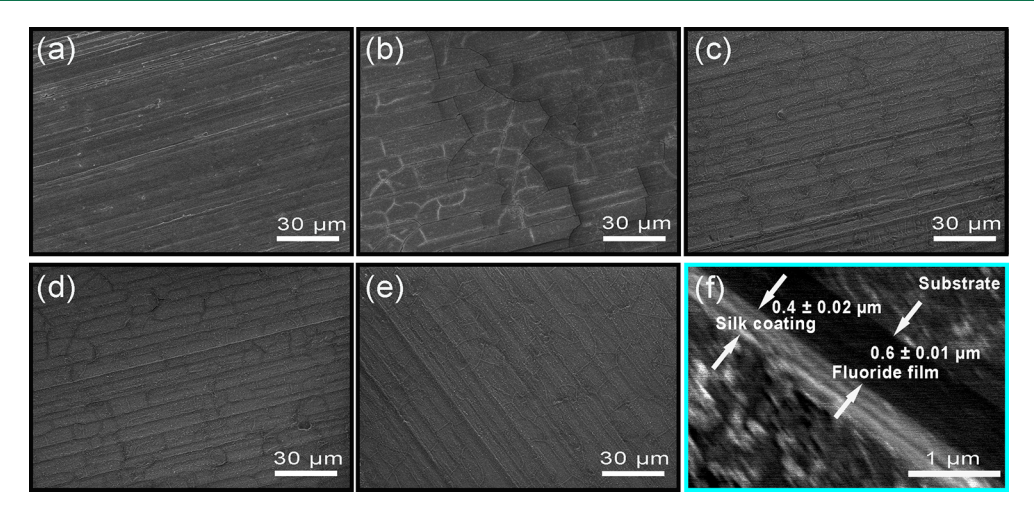


Figure 2. Surface morphologies of (a) bare Mg-1Ca alloy, (b) fluoride pretreatment, (c) silk, (d) Ca/P silk, and (e) Ca, Sr/P silk; (d) cross-sectional morphology of the Ca, Sr/P silk.

the spin-coated samples were dried in a vacuum oven at room temperature.

2.4. Material Characterization. The surface and cross-section morphologies of the samples were investigated by S-4800 field emission scanning electron microscope (FE-SEM; Hitachi) equipped with an energy-dispersive spectrometer (EDS) attachment. The chemical states of all groups were determined by X-ray photoelectron spectroscopy (XPS; AXIS Ultra, Kratos) with Al K α irradiation (hv =1486.71 eV). The functional groups of the silk fibroin films were recognized by Attenuated Total Reflectance-Fourier Transform Infrared analysis (ATR-FTIR, Thermo Fisher). The spectra were recorded from 4000 to 400 cm⁻¹. Peak Fit software was used to fit and calculate the characteristic peak of functional groups. 43 The static contact angle of silk fibroin-coated samples was measured using a contact angle meter equipped with a high-resolution camera (SL200B, Kino, USA) at room temperature (25 °C). The static contact angle was measured by dropwise addition of distilled water (2 mL) onto the sample surface. Each sample was measured in triplicate.

2.5. In Vitro Corrosion Behavior Studies. 2.5.1. Immersion Experiments. The immersion tests were carried out in Hanks' solution (NaCl 8.00 g/L, KCl 0.40 g/L, CaCl₂ 0.14 g/L, NaHCO₃ 0.35 g/L, MgSO₄·7H₂O 0.20 g/L, Na₂HPO₄·12H₂O, 0.12 g/L, KH₂PO₄ 0.06 g/L, pH 7.4) at 37 °C according to ASTM-G31–72. The pH value and hydrogen evolution rate of the solution were monitored during the immersion tests. Three parallel samples were taken in every test. After being immersed for 10 and 30 days, respectively, samples were taken out of the solution, and rinsed with deionized water, then dried in air. The changes of surface morphologies before and after immersion for 10 and 30 days were checked by SEM.

2.5.2. Electrochemical Measurements. Electrochemical measurements were carried out in a standard three-electrode cell in Hanks' solution at 37 °C using an electrochemistry workstation an electrochemistry workstation (PGSTAT 302N, Metrohm Autolab). The samples were served as the working electrode while a saturated calomel electrode (SCE) and a platinum piece were adopted as the reference and counter electrodes, respectively. The exposed area of the working electrode to the electrolyte was 0.41 cm². The electrochemical impedance spectroscopy (EIS) measurement was done with a scanning frequency range from 1×10^5 to 1×10^{-2} Hz with a single amplitude of 10 mV. EIS spectra were shown by Nyquist plots, and were quantitatively simulated using corresponding equivalent circuits. Potentiodynamic polarization scans were performed at a scanning rate of 1 mV/s, and the initial potential was 500 mV below the open circuit potential (OCP). An average of three measurements was taken for each group.

2.6. Cytocompatibility. *2.6.1. Cell Culture and Seeding.* Mouse osteoblast-like cells (MC3T3-E1) were used for the in vitro

biocompatibility measurements. Cells were cultured in α -MEM (minimum essential medium alpha), which contained 10% FBS (fetal bovine serum, HyClone, Beijing), 1% penicillin and streptomycin (HyClone, Beijing), in a humidified incubator with 5% CO₂ at 37 °C. All samples were sterilized in UV radiation for at least 1 h for each side. In the direct cell adhesion, samples were settled in 24-well plates (TCPS; Corning, USA), and 500 µL cell suspensions were seeded in each well at a cell density of 5×10^4 /mL. In the indirect cell experiments, extracts of the samples were used. Each specimen was immersed in non-FBS α -MEM for 3 days with a ratio of 1.25 mL/cm² according to ISO10993-12 to obtain the extracts. The extracts were preserved at 4 °C prior to the experiments. The seeded cells were cultured in 96-well plates (2000 cells per well), 48-well plates (4000 cells per well), and 24-well plates (25 000 cells per well), respectively, for 24 h to allow the attachment of cells. Then, the medium was replaced by extracts with equal volume.

2.6.2. Cell Adhesion. Cells were seeded on the samples directly. After culturing 24 h, the samples were rinsed with PBS for three times and then immersed in 2.5% glutaraldehyde solution for 1 h at room temperature. The samples were then dehydrated in a gradient ethanol/DI water (the concentration of ethanol was 50, 60, 70, 80, 90, 95, and 100%) and each concentration for 10 min. The morphologies of the cells adhered to the surfaces of samples were observed using SEM

2.6.3. Cell Proliferation Assay. Cell viability was evaluated with released extracts employing a mitochondrial activity-based cell counting kit (CCK-8, Dojindo, Japan) according to the manufacturer's instructions. The seeded cells (2000 cells per well) were cultured in 96-well plates. In the meantime, 100 μL of α-MEM alone used as the negative control and 100 μL α-MEM containing 10% DMSO (dimethyl sulfoxide) used as the positive control. Cells were cultured for 3 and 5 days to measurements. At scheduled time points, the medium was replaced by 100 μL of fresh α-MEM with 10% CCK-8 solution and incubated for another 2 h to generate formazan. The spectrophotometric absorbance ([A]) was determined at 450 nm on a microplate spectrophotometer (Bio-Rad, USA). The cell viability was calculated as follows:

%cell viability =
$$\left(\frac{[A]_{\text{sample}} - [A]_{\text{positive}}}{[A]_{\text{negative}} - [A]_{\text{positive}}} \right) 100\%$$
 (3)

2.6.4. Live/Dead Assay. Cells were cultured in 48-well plates for 3 and 5 days with extracts respectively and subjected to live/dead assay. Briefly, cells were washed with PBS several times and then incubated with certain amounts of fluorescent dye (2 mM Calcein AM and 4 mM PI, Live/Dead Cell Stains, Dojindo, Japan) for 20 min in the humidified incubator. The cells were then rinsed twice using PBS, and

ACS Biomaterials Science & Engineering

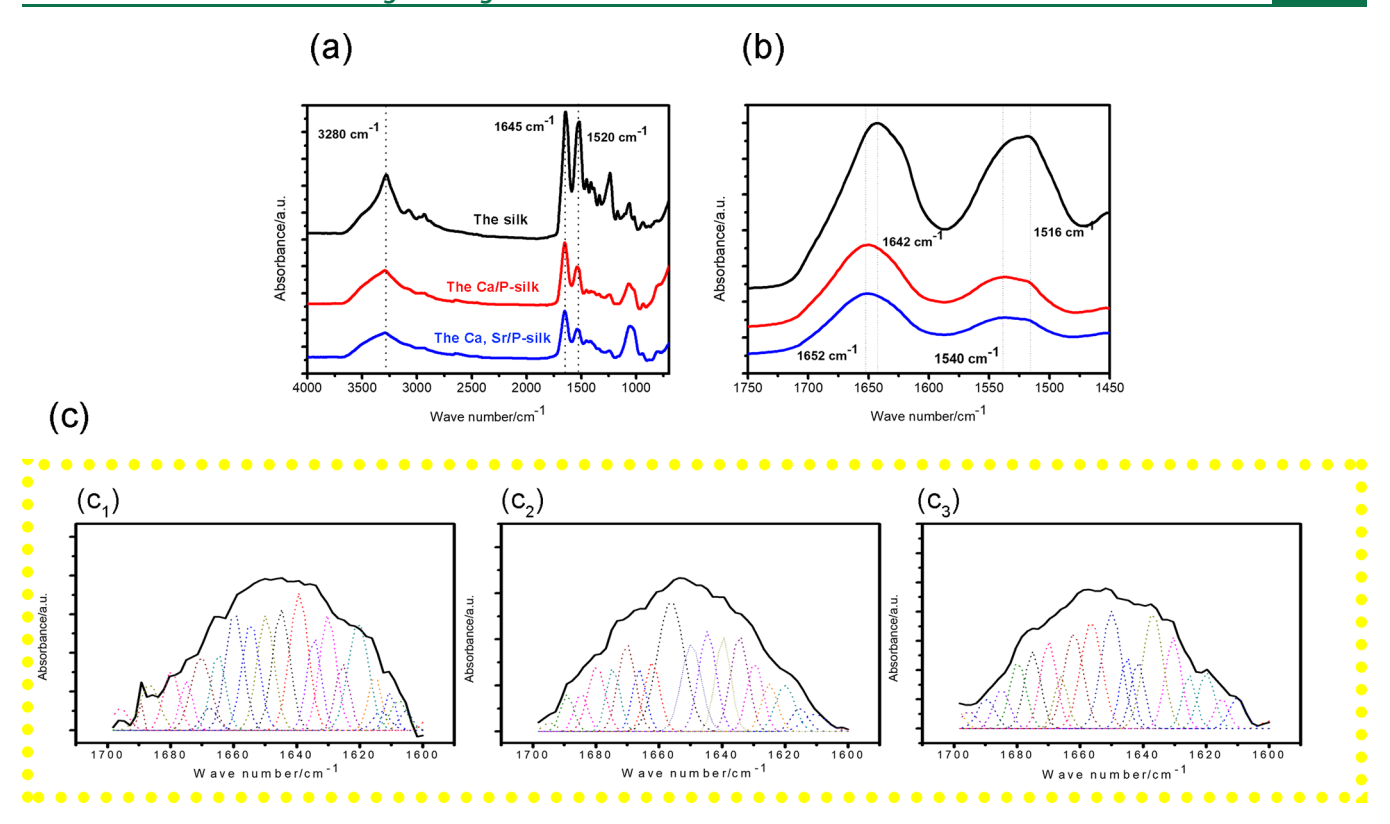


Figure 3. (a)(b) ATR-FTIR spectra of silk-coated samples. (c) Absorbance spectra, amide I, deduced after Fourier self-deconvolution of the $silk(c_1)$, the Ca/P $silk(c_2)$ and the Ca, Sr/P $silk(c_3)$. The heavy line represents the contributions to the amide I band while the dotted lines represent the individual contributions.

visualized using LSCM (laser scanning confocal microscope, Nikon ALR-SI; identical apparatus throughout the experiments).

2.6.5. Cytoskeleton and Cell Spreading. Sterilized glass plates (φ = 10 mm) were put in 24-well plates and the cells were cultured on the plates with the extracts for 12 and 24 h, respectively. Cells were then washed with PBS, fixed using 4% (w/v) paraformaldehyde for 10 min and permeabilized with 0.1% (v/v) Triton X-100 (Sigma) for 7 min. Following this, 1.0% (v/v) FITC-phalloidin (Sigma) was used to stain the cellular actin for 30 min and 1 mg/mL DAPI (Sigma) was used to stain the nuclei for 5 min. Cells were washed for many times and imaged by LSCM.

2.6.6. Osteogenic Differentiation Studies. Alkaline phosphatase (ALP) activity was measured to evaluate the osteogenic differentiation by culturing cells with extracts for 7 and 14 days. Cells were lysed in 1% Triton X-100 using standard freeze thaw cycles. The ALP activity in the lysis was probed spectrophotometrically by measuring the colorimetrical production of p-nitrophenol (p-NP) via p-nitrophenyl phosphate (p-NPP)/endogenous ALP enzymatic reaction, as per manufacturer instructions (Jiancheng, Nanjing, China). The results were normalized against the total intracellular protein content measured by the Micro BCA protein kit and expressed as mM production of p-NP by each gram of protein (mM p-NP/gprot). α -MEM alone was added per well into TCPS as the control, and the cell differentiation activity was calculated with respect to the control as follows:

cell differentiation activity (%) =
$$\left(\frac{[ALP]_{sample}}{[ALP]_{control}}\right)$$
100% (4)

2.7. Statistical Analysis. All data were expressed as the mean \pm standard deviation with n=3 and analyzed using a one-way analysis of variance (ANOVA) followed by Tukey's post hoc tests using SPSS 19.0. The p < 0.05 was considered statistically significant.

3. RESULTS AND DISCUSSION

Figure 2a-e showed the surface morphologies of all groups. The bare Mg-1Ca alloy (Figure 2a) exhibited a typical grooved morphology due to mechanical grinding. After fluoride pretreatment samples showed a surface with many cracks similar to the previous studies. 18 The silk-coated samples exhibited a homogeneous surface and did not have any crack, indicating that the silk fibroin films had covered the Mg-1Ca alloy substrate closely. In addition, the silk coated samples showed a rough surface without any defect, which may be beneficial to cells adhesion at the early stage. It was previously reported that silk fibroin films were brittle and were peeled off from substrate easily,²⁶ but the silk fibroin films in our work displayed a uniform surface morphology and encapsulated substrate completely, which was attributed to the addition of PEG₂₀₀ that had been reported to enhance the toughness.⁴⁴ Moreover, the surface morphologies of silk fibroin films with Ca/P and Ca, Sr/P or not had no significant difference. It indicated that the Ca/P and Ca, Sr/P could diffuse uniformly in the silk fibroin solution which may be attributed to the intermolecular and intramolecular interactions of the Ca/P and Ca, Sr/P with silk fibroin. Importantly, for silk/apatite composites prepared by coprecipitation, the proportion of Ca/P and Ca, Sr/P salts in silk solution exerts appreciable impact on the quality of the resulting films. For example, in fabricating a SF/HA film, only when the HA content was at a low level can the obtained film be smoot, transparent and uniform; otherwise, phase separation would occur.³³ Therefore, given the desirable morphology and uniform distribution of inorganic salts in our films, the Ca/P and Ca, Sr/P amounts

3.1. Surface Morphology and Coating Thickness.

introduced should be suitable.

The cross-sectional SEM image of the Ca, Sr/P silk was shown in Figure 2f. The samples were encapsulated by acrylic resin to keep the sample undestroyed. As measured, the thickness of fluoride film was about $0.63 \pm 0.01~\mu m$ and that of silk fibroin films was approximately $0.42 \pm 0.02~\mu m$.

3.2. Chemical Composition of the Surface. Silk fibroin was one kind of typical protein, which is composed of a heavy chain (325 kDa) and a light chain (25 kDa) connected by a disulfide bond and complexed by small glycoprotein P25 (30 kDa). The main elements of silk fibroin are repeats of the GAGAGS motif.²⁶ ATR-FTIR was used to characterize the functional groups of silk-coated Mg-1Ca alloy, as shown in Figure 3a, b. A broad absorption at 3280 cm⁻¹ appeared in each sample, assigned to O-H from the H2O bind to the surface. 45 The peaks at 1645 and 1520 cm⁻¹ were the amide I (N-H deformation) and amide II (C-N stretching), respectively, characteristic peaks of silk fibroin. 46 Besides, the absorption band at 1035 cm⁻¹ corresponding to v₃ vibration peak of P-O was one of the well-defined peaks of the PO₄³⁻ group emerged.45 Therein, Ca/P and Ca, Sr/P were successfully doped in silk fibroin films, and moreover, with uniform distribution as no phase separation occurred. Additionally, to better interpret the changes in the secondary structures of silk fibroin for the Ca/P silk and the Ca, Sr/P silk, the characteristic bands of amide I adsorption from 1750 to 1450 cm⁻¹ were selected and deconvoluted into several subpeaks (Figure 3c). The proportion of the main secondary structures within the silk fibroin films were thus calculated (Table 2). The percentages of β -sheets (33.0% \pm 1.0%) were

Table 2. Relative Ratio of Second Structures in the Silk, Ca/P Silk, and Ca, Sr/P Silk

| assignment | silk | Ca/P silk | Ca, Sr/P silk |
|--|------------------|------------------|------------------|
| assignment | SHK | Ca/1 Siik | Ca, 51/1 311K |
| side chains (1590–1605 cm ⁻¹) | $3.6\% \pm 0.1$ | $0.1\% \pm 0.2$ | $0.6\% \pm 0.1$ |
| silk II, β -sheets (1610–1635cm ⁻¹ , 1695–1700 cm ⁻¹) | $32.7\% \pm 0.3$ | $33.3\% \pm 0.1$ | $33.1\% \pm 0.1$ |
| random coils (1635–1645 cm ⁻¹) | $18.4\% \pm 0.1$ | $7.2\% \pm 0.1$ | $4.4\% \pm 0.2$ |
| silk I, type II b-turns (1647–1654 cm ⁻¹) | $7.8\% \pm 0.2$ | $17.3\% \pm 0.3$ | $15.8\% \pm 0.1$ |
| α -helices (1658–1664 cm ⁻¹) | $15.7\% \pm 0.1$ | $22.5\% \pm 0.1$ | $22.9\% \pm 0.2$ |
| turns and bends $(1666-1695 \text{ cm}^{-1})$ | $21.8\% \pm 0.1$ | $19.6\% \pm 0.2$ | $23.2\% \pm 0.1$ |

the same in the three groups, resulted in good water stability.⁴⁷ It should be noted that the percentages of random coils, silk I and α -helices varied a lot. Particularly, Ca/P and Ca, Sr/P addition led to 45.7% decrease in the proportion of random coils in comparison to that of pure silk fibroin films (18.4% \pm 0.1%). Moreover, compared to pure silk fibroin films, the proportion of α -helices in the Ca/P silk and the Ca, Sr/P were increased to 22.5% \pm 0.1% and 22.9% \pm 0.2%, respectively, whereas the silk I content increased from $7.8\% \pm 0.2\%$ to $17.3\% \pm 0.3\%$ (Ca/P silk) and $15.8\% \pm 0.1\%$ (Ca, Sr/P silk). In this study, the high pH of silk fibroin (10 \pm 0.5) helped maintain the high proportion of random coils in the pure silk fibroin films. However, the spinning process can give rise to the proportion of β -sheets.²⁰ Especially, the random coils were negatively charged in the solution. When Ca/P and Ca, Sr/P were doped in silk fibroin, the Ca²⁺ and Sr²⁺ would reverse the charges of the random coils and force it to fold and form silk I

and α -helices (Figure 1 (inset)). The latter were water-stable structures more suitable for biomaterials application, ^{27,43} which may benefit both corrosion resistance and cytocompatibility of Mg–Ca substrate.

XPS was employed to identify the chemical valence information on films constituents. The survey spectrum (Figure 4a) showed the main elements on the surface of each sample. The resulted revealed that the silk fibroin films were coated on the substrate successfully. It was dense due to not detecting the fluorine on the silk fibroin-coated samples.

In addition, Ca, P, and Sr elements were detected for the Ca/P silk and the Ca, Sr/P silk. The ratio of Ca/P was 4.15 for Ca/P silk fibroin and the ratio of (Ca+Sr)/P for the Ca, Sr/P silk was 4.89. It was found that the ratios of Ca/P and (Ca+Sr)/P were higher than the initial solution ratios. It may be contributed to the positive ions were more likely to bind to silk fibroin because of the electrostatic interactions. Besides, the core-level spectra for C 1s, O 1s, and N 1s of the Ca, Sr/P silk were decomposed. C 1s showed the characteristic peaks at 284 (C-S), 286 (C-H), and 288 (C=O). For the O 1s core-level spectrum, the peaks belonged to O=C (531 eV), O=C (531.5 eV), and O-H (532.5). The N 1s spectrum was fitted into two components, namely N-H (400 eV) and N-C (399.5 eV). All the characteristic peaks corresponded to functional groups within silk fibroin, suggesting peptide bond, 48 hydroxyl, 49 and disulfide bond, 50 respectively.

3.3. Contact Angles. The sensitivity of contact angle (CA) measurements was utilized to assess the hydrophily of the silk fibroin-coated groups (Figure 5). The lower the CA was, the more hydrophilic the surface was. Initially, the pure silk fibroin films was relatively hydrophilic (19.5 \pm 0.6°). The CAs of the Ca/P silk and the Ca, Sr/P silk were increased by (32.0 \pm 0.1°) and (37.1 \pm 0.6°), respectively. The data in section 3.2 indicated that when Ca/P and Ca, Sr/P were added in silk fibroin, the Ca²⁺ and Sr²⁺ induced the second structure of silk fibroin from random coils to α -helices, and thus decreased the hydrophily and improved the stability of the films in solution environment. This would endow the films with a physical barrier for the substrate when the sample was used in a physiological environment.

3.4. In Vitro Corrosion. 3.4.1. Surface Corrosion Morphology. Samples of all groups were immersed in Hanks' solution for 10 and 30 days, respectively. The surface morphologies after immersion were shown in Figure 6. At day 10, cracks were noticed in all samples, but the corrosion morphologies were significant different. Bulk corrosion products were found on the bare Mg-1Ca alloy, whereas the surface-modified Mg-1Ca alloy samples only showed microcracks. Moreover, after being immersed for 30 days, the untreated Mg-1Ca alloy samples underwent much severer corrosion, as the cracks on the surface became broader and deeper. The fluoride pretreated Mg-1Ca alloy specimen also had obvious cracks on the substrate. For the three groups with silk, despite cracks presenting in all, the Ca/P silk and the Ca, Sr/P silk displayed smaller cracks than did pure silk fibroin films. These results possibly arise from the fact that random coils in silk fibroin were changed to more stable silk I and α helices. The EDS results of immersion for 30 days matched well with the surface morphologies of specimens. As shown in Table 3, the main corrosion products of all samples were carbonate and phosphate. The Sr was undetectable, probably due to continuing release and slow degradation of the silk fibroin films within 30 days. In addition, the surface of silk

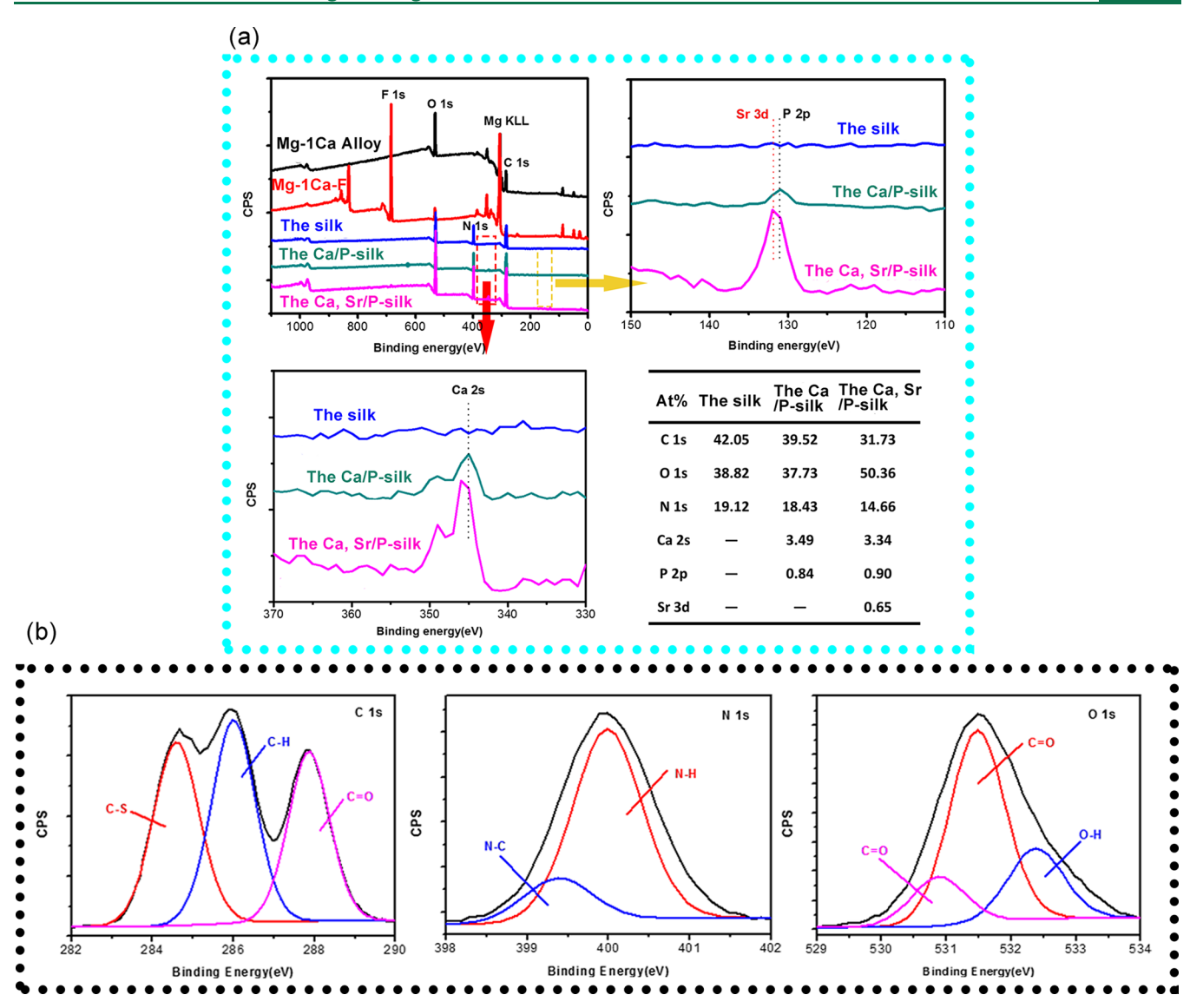


Figure 4. XPS results comprising (a) a survey spectrum and (b) corresponding core-level sepctra for C 1s, N 1s, and O 1s.

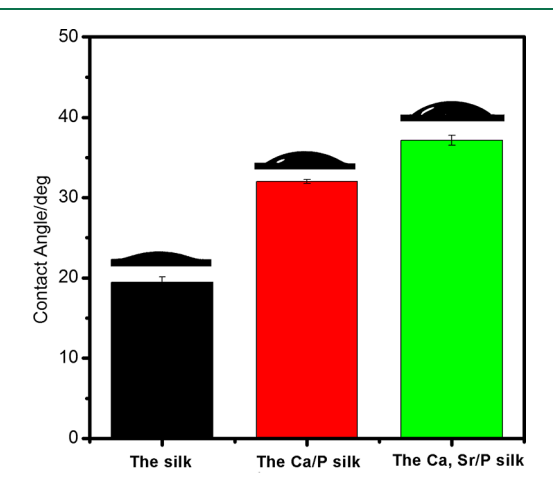


Figure 5. Contact angles of silk fibroin-coated samples.

coated samples contained more fluoride originating from fluorite pretreatment. The immersion tests revealed that the bare Mg-1Ca alloy had a poor corrosion resistance, and the fluoride pretreatment and silk fibroin films exhibited a protective effect. Even being immersed for 30 days, the substrates of the silk fibroin films coated samples were integrate and only the outer silk fibroin films were dissolved. It implied that the composite films might prolong the corrosion time to fit the bone healing process.

3.4.2. Hydrogen Evolution Volume and pH Value. Figure 7 presented the variation in the hydrogen evolution volume and pH value during the immersion period of all experimental groups. Immersed for 10 days, the Ca, Sr/P silk hardly released hydrogen, but the bare Mg-1Ca alloy released speedily during the period (Figure 7a). Meanwhile, as shown in Figure 7b, the pH values result was in accordance with the variation of hydrogen evolution volume. When the immersion finished, the pH value of the Ca, Sr/P silk was about 7.82, whereas the bare Mg-1Ca was approximated to 10.00. Combining the hydrogen evolution volume and pH values results, it revealed the surfacemodified Mg-1Ca alloy samples were hardly ever corroded, whereas the bare Mg-1Ca alloy sample corroded speedily after being immersed for 10 days. It concurred with the surface morphologies immersing for 10 days. The bare Mg-1Ca alloy degraded quickly, thus it released hydrogen fast and was accompanied by increasing pH values. The surface-modified

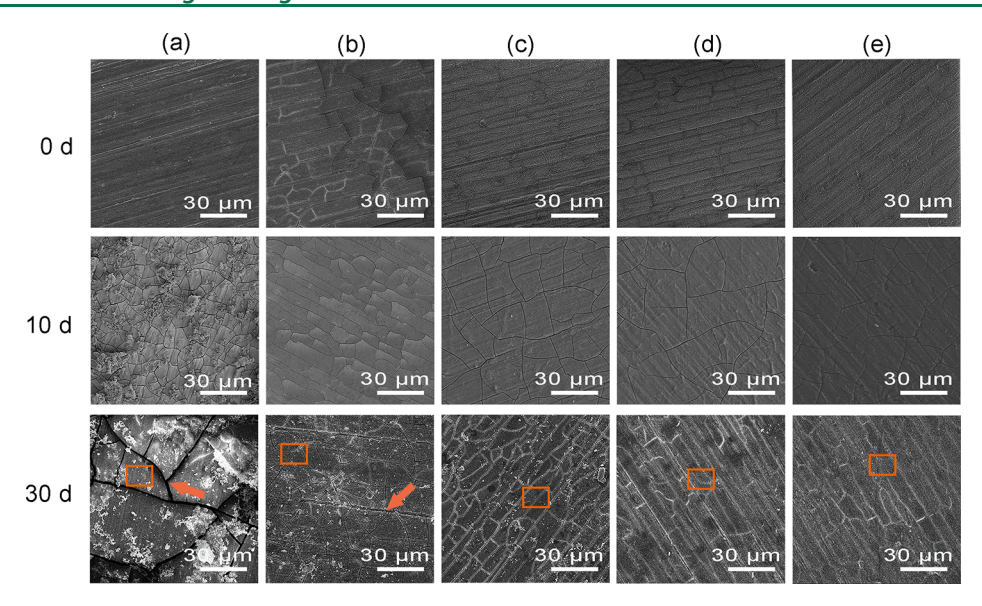


Figure 6. Surface morphology of (a) bare Mg-1Ca alloy, (b) fluoride pretreatment, (c) pure silk films, (d) Ca/P silk, and (e) Ca, Sr/P silk, before and after immersion.

Table 3. EDS Results of Immersion for 30 Days

| | | | at. % | | |
|---------|--------|----------|-------|-----------|---------------|
| element | Mg-1Ca | Mg-1Ca-F | silk | Ca/P silk | Ca, Sr/P silk |
| С | 9.06 | 9.56 | 11.73 | 7.68 | 3.05 |
| O | 81.84 | 54.35 | 36.95 | 38.68 | 25.23 |
| P | | 7.45 | 5.91 | 7.18 | 4.94 |
| Mg | 3.13 | 4.07 | 7.66 | 7.66 | 14.64 |
| Ca | 2.94 | 6.68 | 4.52 | 5.58 | 2.99 |
| F | | 16.85 | 32.75 | 32.13 | 44.49 |

Mg-1Ca alloy specimens just showed cracks but hardly degraded, hence the releasing hydrogen and pH value did not change much. On other hand, the all silk fibroin-coated samples improved the corrosion resistance, but the Ca/P silk and the Ca, Sr/P silk enhanced the corrosion resistance. This result supported that the Ca, Sr/P silk got a more stable structure, which would be a preferable barrier to improving the corrosion resistance.

3.4.3. Electrochemical Measurements. EIS is a nondestructive and powerful technique in assessment of corrosion resistance properties corrosion mechanism. Figure 8a shows the Nyquist plots of EIS spectra (spots) and EIS fitting (solid lines) by the proposed corresponding ECs (equivalent circuits). The EIS response of the bare Mg-1Ca alloy was fitted with one time constant (Figure 8c1). It could be conducted that only one kinetic process occurred during the corrosion process of the bare Mg-1Ca alloy. As such, the equivalent circuit $R_s(R_{ct}Q_{dl})$ presented in Figure 8c was used to analyze the impedance spectra obtained in this work. In this circuit, R_S represented the corrosion resistance of the Hanks' solution, whereas R_{ct} and Q_{dl} represented charge transfer resistance and the double layer formed in the sampleelectrolyte interface, respectively. As for the modified groups, the EC was expressed as $R_s(R_{\rm ct}Q_{\rm dl})(R_{\rm m}Q_{\rm m})$, in accordance with EIS analysis reveal spectra described by two time constants, where $R_{\rm m}$ and $Q_{\rm m}$ were identified as the resistance and capacitance pertaining to the surface films, respectively. The

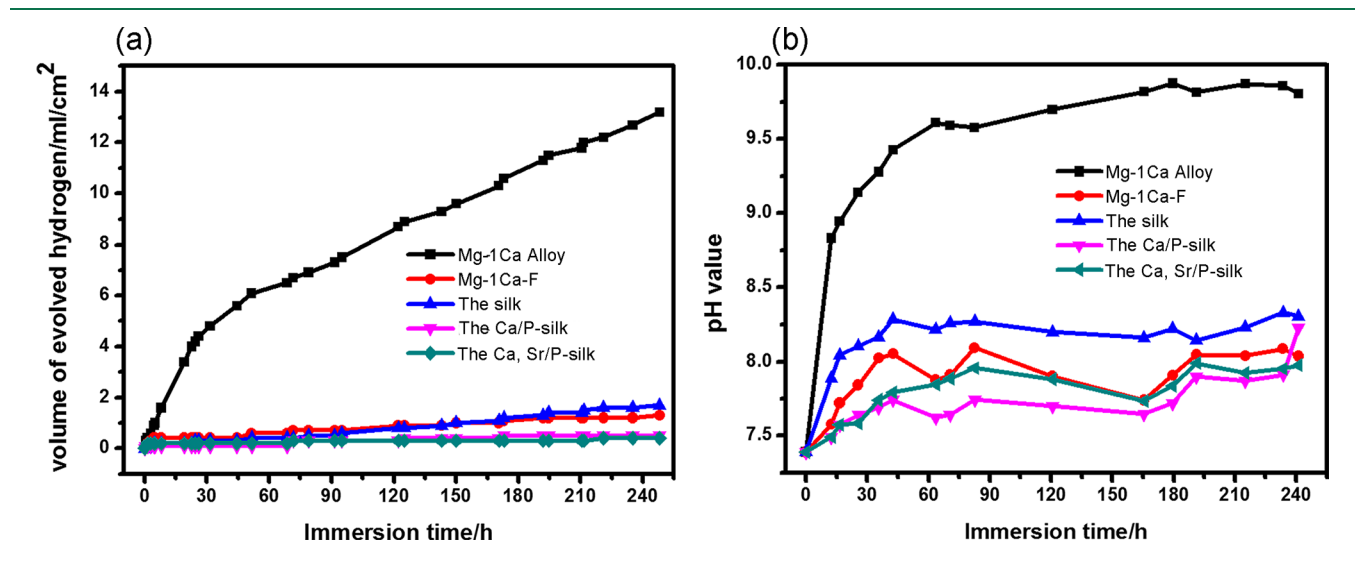


Figure 7. Variation of (a) hydrogen evolution volume and (b) pH values of each group samples during immersion in Hanks' solution for 10 days.

ACS Biomaterials Science & Engineering

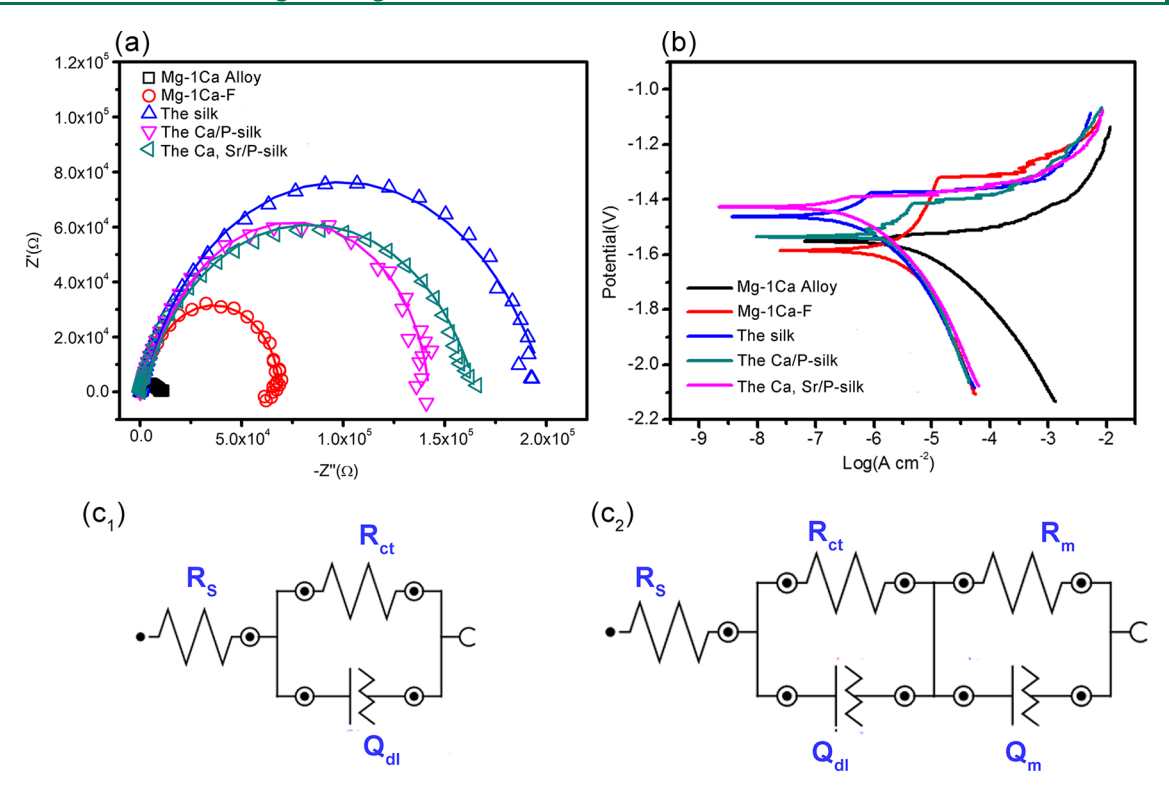


Figure 8. (a) Nyquist plots, (b) potentiodynamic polarization curves of the five groups, and equivalent circuit model for fitting the experimentally obtained impedance data of: (c_1) bare Mg-1Ca alloy, (c_2) specimen after surface modification (fluoride pretreatment and three silk film-coated groups).

Table 4. Electrochemical IE and EIS Fitted Parameters for (a) Bare Mg-1Ca Alloy, (b) Fluoride Pretreatment, (c) Silk, (d) Ca/P Silk, and (e) Ca, Sr/P Silk

| sample | $E_{\rm corr}$ (V) | $I_{\rm corr}~(\mu{\rm A~cm}^{-2})$ | $R_{\rm s}~(\Omega~{\rm cm}^2)$ | $R_{\rm ct}~({\rm k}\Omega~{\rm cm}^2)$ | $Q_{\rm dl}~(\mu {\rm F~s}^{n-1}~{\rm cm}^{-2})$ | n_1 | $R_{\rm m}~({\rm k}\Omega~{\rm cm}^2)$ | $Q_{\rm m} \ (\mu {\rm F \ s}^{n-1} \ {\rm cm}^{-2})$ | n_2 |
|--------|--------------------|-------------------------------------|---------------------------------|---|--|-------|--|---|-------|
| a | 1.5516 | 13.4 | 77.68 | 4.21 | 52.75 | 0.66 | | | |
| b | 1.5850 | 11.2 | 65.19 | 26.16 | 4.93 | 0.98 | 1.25 | 30.53 | 0.72 |
| c | 1.4617 | 0.76 | 76.01 | 77.35 | 8.67 | 0.86 | 10.76 | 67.98 | 0.38 |
| d | 1.5358 | 0.20 | 71.34 | 47.28 | 9.83 | 0.97 | 10.29 | 25.89 | 0.71 |
| e | 1.4271 | 0.49 | 75.03 | 56.53 | 9.88 | 0.83 | 10.46 | 64.23 | 0.70 |

fitted parameters of the impedance spectra were summarized in Table 4. The value of the reaction resistance $R_{\rm ct}$ was characteristic of the corrosion resistance of the surface coatings and was worth comparing to determine the relative protective effect. The $R_{\rm ct}$ value of silk coated samples were more than 1 order of magnitude larger than that of the bare Mg-1Ca alloy and twice as fluoride pretreatment.

The representative Tafel curves were provided in Figure 8b. The surface-modified Mg-1Ca alloy samples showed reduced kinetics of both anodic and cathodic reactions than that of bare Mg-1Ca alloy sample. After surface modification, the corrosion current density of the Mg-1Ca alloy samples decreased. For the silk fibroin films, the corrosion current density decreased nearly 2 orders of magnitude whereas fluoride pretreatment decreased approximately 1 order of magnitude. The $E_{\rm corr}$ and $I_{\rm corr}$ values are summarized in Table 4. The results indicated distinctly that the silk fibroin films exhibited a better protective function as reflected from their more positive $E_{\rm corr}$ and lower $I_{\rm corr}$ values. In previous studies, Sun et al. researched two colloidal particles coated on Mg-1Ca alloy, 16,52 the $I_{\rm corr}$ just achieved 9.98×10^{-5} A/cm², our study could reduce the $I_{\rm corr}$ at least by 2 orders of magnitude. Combining the EIS and Tafel curves data, it provided a powerful evidence that both the

fluoride pretreatment and silk fibroin films improved the corrosion resistance and the silk fibroin films could strengthen the resistance by providing a densified coverage.

3.4.4. Corrosion Behavior in Vitro. To further understand the corrosion behavior of the Ca, Sr/P silk in vitro, the samples were immersed in Hanks' solution at various times and the surface properties were studied. The EIS results are shown in Figure 9a, including the Nyquist plots of EIS spectra (spots) and EIS fitting (solid lines) by the proposed corresponding EC (equivalent circuit). The sample immersed at various time shared the same EC with three time constants, whereas the sample before immersion had two time constant (Figure $8c_2$). The EC was expressed as $R_s(R_1Q_1)(R_2Q_2)(R_3Q_3(R_1L))$ (Figure 9c), and the values of corresponding elements are summarized in Table 5. To quantify the corrosion resistance of the sample at different times, we calculated the polarization resistance (R_p) , because the higher the R_p value, the lower the corrosion rate of the corroding material.⁵³ Generally, the polarization resistance was defined as the difference between the real impedance of the Nyquist plot when the frequency was equal to zero with the solution resistance $(R_s)^{.54}$ By this definition, we calculated R_p with the following equation for the corresponding model:

ACS Biomaterials Science & Engineering

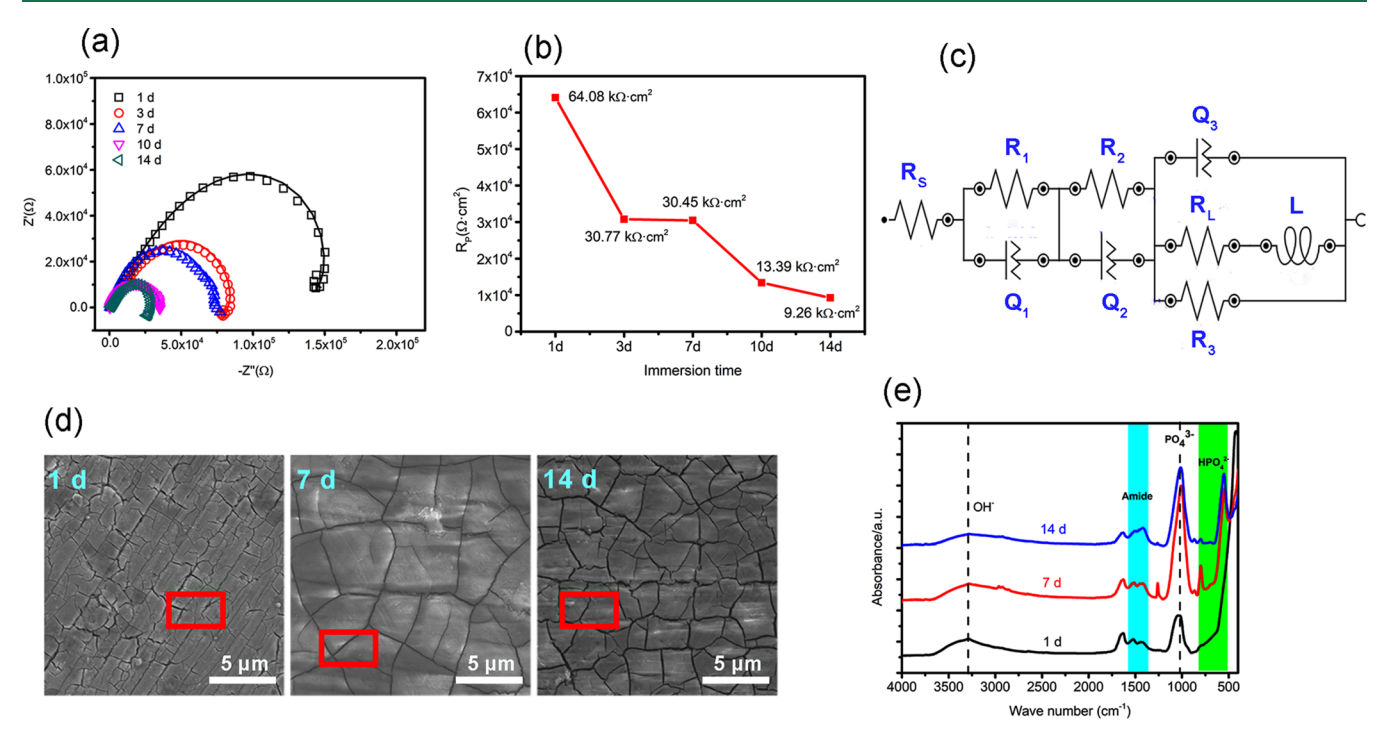


Figure 9. (a) EIS and fitting results, (b) polarization resistance, (c) equivalent circuit model, (d) surface morphology by SEM image, and (e) ATR-FTIR spectra of the Ca, Sr/P silk immersion in Hanks' solution at various time.

Table 5. EIS Fitted Parameters for the Ca, Sr/P Silk Immersion in Hanks' Solution at Various Times

| immersion time (days) | $(\Omega \text{ cm}^2)$ | $R_{\rm ct} \over ({\rm k}\Omega~{\rm cm}^2)$ | $(\mu F s^{Q_{\text{dl}}} cm^{-2})$ | n_1 | $\frac{R_{\rm m}}{({ m k}\Omega~{ m cm}^2)}$ | $(\mu F s^{n-1} \cdot cm^{-2})$ | n_2 | $\frac{R_{\rm o}}{({ m k}\Omega~{ m cm}^2)}$ | $(\mu Fs^{n-1} cm^{-2})$ | n_3 | $\frac{R_{\rm L}}{({ m k}\Omega~{ m cm}^2)}$ | L (kH cm ⁻² |
|--------------------------|-------------------------|---|-------------------------------------|-------|--|---------------------------------|-------|--|--------------------------|-------|--|------------------------|
| 1 | 34.37 | 239.36 | 1.39 | 0.68 | 60.77 | 8.24 | 0.74 | 80.81 | 11.78 | 0.49 | 8.28 | 225.12 |
| 3 | 80.77 | 147.27 | 0.15 | 0.94 | 29.79 | 5.60 | 0.79 | 20.01 | 7.74 | 0.52 | 2.27 | 124.96 |
| 7 | 30.18 | 272.66 | 10.69 | 0.50 | 20.11 | 4.70 | 0.77 | 0.71 | 8.73 | 0.76 | 0.22 | 25.02 |
| 10 | 121.03 | 175.08 | 11.59 | 0.88 | 13.19 | 11.75 | 0.69 | 37.49 | 12.33 | 0.93 | 0.06 | 80.71 |
| 14 | 35.30 | 301.57 | 0.84 | 0.63 | 8.94 | 12.25 | 0.87 | 90.94 | 27.41 | 0.47 | 0.04 | 55.70 |

$$\frac{1}{R_{\rm p}} = \frac{1}{R_1 + R_2 + (R_3^{-1} + R_{\rm L}^{-1})^{-1}}$$
 (5)

Figure 9b showed that the polarization resistance of the sample immersed in Hanks' solution from 1 to 14 days. The $R_{\rm P}$ was reduced when the immersion time was prolonged and had two steps down (3 and 10 days, respectively). When immersed for 1 day, narrow cracks appeared on the surface (Figure 9d). When immersed for 7 and 14 days, the cracks were more broad. The EDS results (Table 6) showed high content of C when immersion for 1 day (34.47 at. %), but a lower conent of C when immersed for 7 days (25.54 at. %) and 14 days (4.14

Table 6. EDS Results of the Ca, Sr/P Silk Immersion for 1, 7, and 14 days

| | | at. % | |
|---------|-------|--------|---------|
| element | 1 day | 7 days | 14 days |
| С | 34.47 | 25.54 | 4.14 |
| O | 36.68 | 21.03 | 10.25 |
| N | 13.68 | 8.01 | 1.99 |
| P | 7.52 | 8.33 | 16.96 |
| Mg | 1.98 | 9.92 | 10.71 |
| Ca | 5.25 | 7.07 | 19.73 |
| Sr | 0.42 | | |
| F | | 20.10 | 36.22 |

at. %), which implied the reduction of the films on the surface, due to C element as skeleton of silk fibroin. The FTIR results were in accordance with the EDS. Combining the EIS results, surface morphology changes and surface chemical composition results, it suggested once the sample immersed in Hanks' solution, the outer films swelled and the cracks appeared, resulting in another interface appearing. When immersing after 7 days, the cracks got broad, fluoride film exposed, and phosphate precipitated on the surface. After immersing for 14 days, much less Ca, Sr/P silk existed, whereas the larger the fluoride surface exposed, the more phosphate precipitated.

The degradation mechanism of the Ca, Sr/P silk might be inferred as follows. At the initial stage of immersion, the films swelled. The swelling films were accompanied by volume expansion, thus cracks showed up on the surface. Because of the cracks on the surface, one more interface appeared but did not change during immersion, which illustrated that corrosion happened only on the surface, and the Mg-1Ca alloy substrate was not corroded, hence the pH values and the amount of releasing hydrogen had a slight change. It was inferred that the Ca, Sr/P silk could provide protection for the substrate during 14 days, even though the protection ability gradually reduced. After immersing for 30 days, the films disappeared and the fluoride pretreatment film was fully exposed to the outside; the Mg-1Ca alloy substrate might be corroded further but the integrity of substrate could be maintained even after being

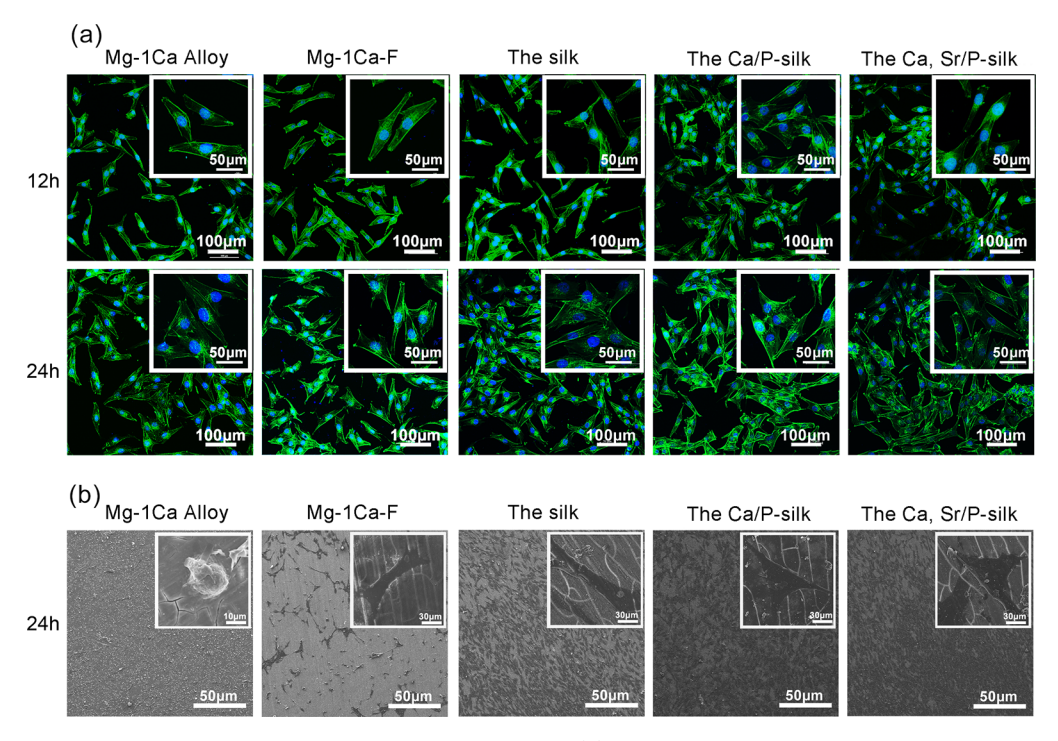


Figure 10. (a) Actin nucleus costaining of cells cultured for 12 and 24 h, and (b) cell morphologies after culturing for 24 h on bare Mg-1Ca alloy, fluoride pretreatment, pure silk films, the Ca/P silk, and the Ca, Sr/P silk.

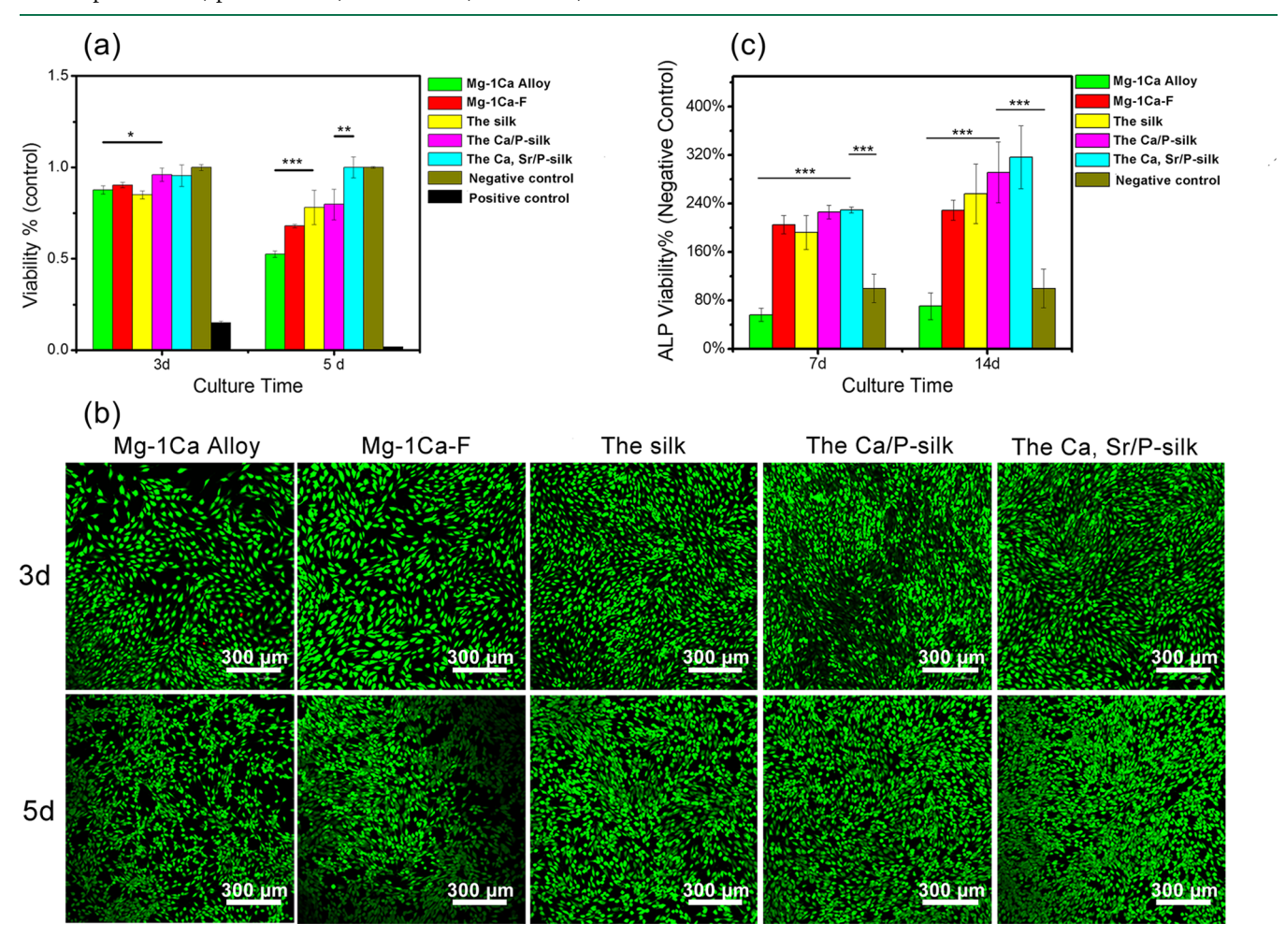


Figure 11. Viability of cells cultured in the extracts of each samples at 3 and 5 days by (a) the CCK-8 assay kit and (b) live/dead staining. (c) ALP activity of cells cultured for 7 and 14 days. * represents p < 0.05, **represents p < 0.01, ***represents p < 0.001.

immersed for a longer time. In addition, more and more phosphate precipitated, which could be barrier to the corrosion medium, as well as endow bioactive for the substrate. In the past few years, many natural and synthetic polymers, like PLA, PGA, PLGA, PEI, have been applied to the surface of Mg alloys to improve the corrosion resistance and surface bioactivity, due to their versatile chemical and physical properties. 55,56 As revealed by previous investigations, polymers like PLGA would degrade by hydrolyzing the ester bond to lactic and glycolic acid monomers. Because of the autocatalytic effect of degradable polymers, the acidic degradation products wherein can further accelerate degradation of remaining polymers. Once the degraded products diffuse to the surface of the substrate, it accelerates the corrosion of the Mg alloy substrate. In addition, previous studies revealed that polyelectrolyte layers, especially those derived from natural polysaccharides, were porous, which allowed for the rapid diffusion of water and for ions to penetrate through them, and thus cannot provide any corrosion protection for substrate. These phenomena did not exist on the Ca, Sr/P silk. Noticeably, although Ca, Sr/ P doped in the silk fibroin, they induced more α -helices from random coils. This structure transformation could be a preferable barrier for the substrate in the physiological environment.

3.5. Cytocompatibility. 3.5.1. Cell Morphology and Spreading. The MC3T3-E1 cells were cultured in extracts for 12 and 24 h respectively and stained with DAPI and FITCphalloidin, as shown in Figure 10a. After being cultured for 12 h, the numbers of cells in different groups varied significantly. In addition, the silk fibroin-coated Mg-1Ca alloy groups had more cells than fluoride-pretreated Mg-1Ca alloy group. After being cultured for 24 h, cells propagated. The number of cells in all groups increased, and the silk fibroin-coated groups showed the largest number of cells among all groups. At higher magnification, cells on silk fibroin-coated groups appeared well spread out and extend in numerous directions and exhibiting a rearranged while cells on the bare Mg-1Ca alloy and fluoridepretreated Mg-1Ca alloy became elongated. The results revealed that silk fibroin was good for the cells at the early stage to spread and propagate, which was the base for the cells' propagation and differentiation.

3.5.2. Cell Adhesion. Cells were cultured on samples directly for 24 h and observed by SEM. The low/highmagnification images of all groups are shown in Figure 10b. As implied, on bare Mg-1Ca alloy, few cells adhered on the surface, exhibiting spherical shape morphology. For the other four groups, cells showed spreading shape when adhered on samples and the filopodia could be found at high magnification. In comparison to other groups, silk fibroincoated Mg-1Ca alloy samples not only exhibited better effect on cell adhesion but also promoted the cell spreading on the surface. Due to the fast corrosion rate, the bare Mg-1Ca alloy produced a high alkaline environment that was harmful to the cells adhesion. Surface-modified Mg-1Ca alloy samples had slowed down the corrosion rate, hence cells could adhere to the surface well. Compared with the fluoride pretreatment, the surface of silk fibroin-coated Mg-1Ca alloy samples could enhance cell adhesion, and although Ca/P and Ca, Sr/P were added in silk fibroin films, it indicated the surface was preferable for cells.

3.5.3. Cytotoxicity. The CCK-8 assay kit results after incubating cells in extracts for 3 and 5 days are presented in

Figure 11a, cells cultured on TCP served as control. At day 3, the difference was not significant; the viabilities for the Ca/P silk and the Ca, Sr/P silk extracts were 95% \pm 5%, but the other three groups were just $85\% \pm 2\%$ (relative to TCPS). At day 5, the viability for the Ca, Sr/P silk was the best and outmatched the TCPS, whereas the viabilities for uncoated, fluoride-pretreated and pure silk fibroin films groups were 52% \pm 1%, 67% \pm 0.9%, and 78% \pm 9%, respectively. In Figure 11b, showing results after culturing for 3 and 5 days, the results shown by live/dead staining images coincide well with those revealed with CCK-8 kit. Combining the results of two measurements, it revealed that silk fibroin-coated Mg-1Ca alloy samples were better than the bare Mg-1Ca alloy and fluoridepretreated Mg-1Ca alloy groups in cells proliferation, which is attributed to the good biocompatibility of silk fibroin. Moreover, the Ca, Sr/P silk exhibited the best performance, maybe due to the changes of the second structures.

3.5.4. Osteogenic Differentiation. ALP activity was a hallmark for osteogenic differentiation potential of cells. MC3T3-E1 cells were seeded for 7 and 14 days and the ALP activity were measured. As illustrated in Figure 11c, cells cultured with α -MEM was set as negative control, after being cultured for 7 days, the ALP activity of the surface-modified groups were much higher than the bare Mg-1Ca alloy and twice that of the TCPS. After being cultured for 14 days, the Ca, Sr/P silk showed the highest ALP activity and was nearly triple that of the negative control. Overall, the silk-coated Mg-1Ca alloy groups had higher ALP activity than that of the bare Mg-1Ca alloy, fluoride-pretreated group, and the negative control. The results revealed the ALP activity of silk fibroin film-coated groups was higher than that of the other groups, due to the admirable osteogenic activity of silk fibroin.²⁹ The Ca, Sr/P silk showed the highest ALP activity, which might relate to the addition of Ca, Sr/P and the transformation of the second structure of silk fibroin.

3.5.5. Mechanisms of Cell Behavior. Overall, the Ca, Sr/P silk fibroin composite films, which were designed to mimic the ECM, endowed the better cytocompatibility and excellent bioactivity for Mg-1Ca alloy. To assist understanding, we show in Figure 12 the possible factors affecting cell behaviors upon material exposure. On the one hand, the bare Mg-1Ca alloy had a poor corrosion resistance; rapid corrosion was accompanied by unduly high pH values, Mg²⁺ concentration, hydrogen bubbles, and bulk corrosion products. High pH values could denature membrane proteins, thereby destroying the disabling active ionic transport. Increased Mg2+ concentration might alter the osmotic pressure of the cell membrane, 5,58 breaking the ion channels and F-actin with focal adhesion (indicated in Figure 12a, parts a₁ and a₅). Consecutively generated hydrogen would frustrate cells' attempts to anchor. In the meantime, the large amounts of generated corrosion products with sharp morphologies played the role of mechanical/physical means of damage to cells⁶ (shown in Figure 12a, the part of a2). Nevertheless, for modified groups, preferable corrosion resistance prevented the cells from the damage, thus fluoride-treated and silk-coated samples had a better cytocompatibility than bare Mg-1Ca alloy.

Noticeably, the Ca, Sr/P silk sample significantly enhanced the cells biological responses among the surface-modified groups. Four factors could account for the phenomenon. Foremost, the preferable corrosion resistance of the sample prevented the cells from the damage as discussed previously (as Figure 12b, parts b₁ and b₅). Moreover, silk fibroin was

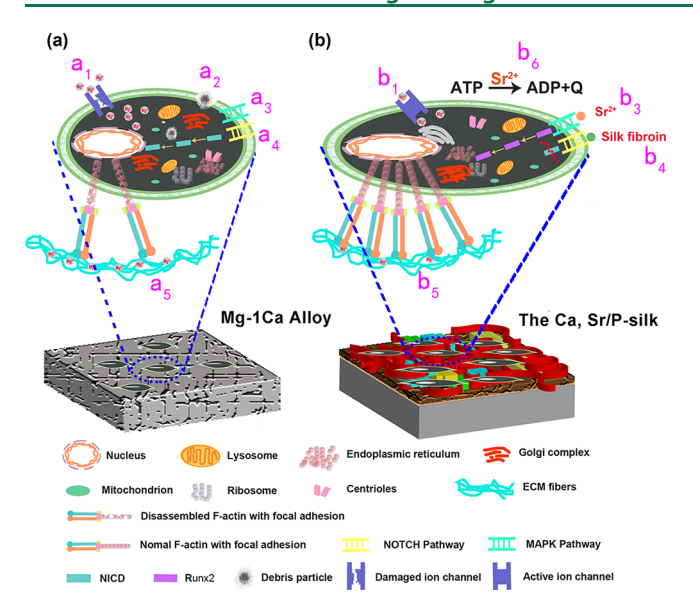


Figure 12. Scheme displaying the possible factors affecting cell behaviors on (a) bare Mg-1Ca alloy and (b) the Ca, Sr/P silk surfaces. The involved processes were labeled as a_1 , a_2 , a_3 ..., and b_1 , b_2 , b_3 ..., respectively.

considered as a promising matrix for bone regeneration, because of the ability of osteogenesis regulation. It was said that silk fibroin enhanced expression of ALP by significantly downregulating Notch signaling cascade, which was responsible for regulating general bone development and remodeling²⁹ (shown in Figure 12b, part b₄). Besides, the hybrid silk fibroin and inorganic salts was a good match of the composite of ECM. This special composite films may be more attractive for osteoblast. Furthermore, the addition of Ca, Sr/P induced the random coils of silk fibroin to α -helices, which was a more stable structure. Additionally, except for Ca/P, which was the inorganic composite in bone and relevant to osteogenesis, 59 Sr, one of trace elements in the human body, was of benefit in enhancing bioactivity and biocompatibility. Sr2+ was related to the breakage of high-energy anhydride linkages in the ATP (adenosine triphosphate), so the energy from the breakage of bonds could be used by the cells to proliferate³⁸ (shown in Figure 12b, part b₆). Besides, Sr²⁺ can promote osteogenic differentiation through activating MAPK signaling pathway and the downstream transcription factor Runx2⁵⁰ (as in Figure 12b, part b₃). Associating with above factors, we inferred that the Ca, Sr/P silk had a splendid cytocompatibility and osteogenesis activity.

In comparison to the previous surface modification methods on Mg-1Ca alloy (Table 7), this work did a comprehensive evaluation for the biocompatibility and bioactivity of materials and showed a much better effect on osteoblast. The results were supplied more evidence to illuminate the excellent

biocompatibility and bioactivity of the Ca, Sr/P silk fibroin composite films on Mg-1Ca alloy.

4. CONCLUSIONS

In this work, bone ECM-like Ca, Sr/P silk fibroin composite films were established on fluoride pretreated Mg-1Ca via spin-coating to improve the corrosion resistance, biocompatibility and osteogenic potential. The introduction of Ca, Sr/P into the films altered the secondary structures of silk fibroin. In vitro corrosion tests including immersion experiments and electrochemical measurements confirmed that the composite films acted as an effective barrier to retard substrate corrosion significantly. Furthermore, the cytocompatibility and ontogenetic performance of the coated material were improved noticeably regarding the adhesion and proliferation, cytoskeleton development and differentiation of MC3T3-E1 cells in vitro. This work provides a new candidate surface modification method for magnesium and its alloys, as well as offers possible mechanisms of the material degradation and cell behaviors.

AUTHOR INFORMATION

Corresponding Authors

*E-mail: chengyan@pku.edu.cn. *E-mail: yfzheng@pku.edu.cn.

ORCID ®

Ming Li: 0000-0001-5823-8108 Yan Cheng: 0000-0001-7956-9395 Yufeng Zheng: 0000-0002-7402-9979

Author Contributions

P.X., Y.F.Z., and Y.C. designed and conducted experiments for surface modification, the in vitro degradation experiments, and the in vitro cell assays. P.X., Z.J.J, M.L., W.H.Z., and J.L.Y. performed the characterizations and analyzed data. Y.H.W. prepared the extruded Mg-1Ca alloy. All the authors contributed to the writing of manuscript.

Funding

This work was supported by National Natural Science Foundation of China (Grant 51431002 and 31170909), NSFC/RGC Joint Research Scheme (Grant 51361165101 and 5161101031), National Key Research and Development Program of China (2016YFC1102402), and NSFC-RFBR Cooperation Project (Grant 51611130054).

Note:

The authors declare no competing financial interest.

■ REFERENCES

(1) Staiger, M. P.; Pietak, A. M.; Huadmai, J.; Dias, G. Magnesium and its alloys as orthopedic biomaterials: a review. *Biomaterials* **2006**, 27 (9), 1728–1734.

Table 7. Comparison of Biocompatibility Evaluations in the Works of Mg-1Ca Alloys with Surface Modification

| | method | cells | adhesion | cytoskeleton (h) | proliferation (days) | differentiation (days) |
|--------------------------|--------------------------|----------------|----------|------------------|----------------------|------------------------|
| this work | | | 1 day | 12, 24 | 3, 5 | 7,14 |
| Gu et al. ⁶¹ | MAO^a | MG63 | 5 days | | 1, 3, 5 | 5 |
| Li et al. ¹⁸ | MgF_2 | MG63, MC3T3-E1 | 3 days | | | |
| Sun et al. ¹⁶ | γ-PGA-g-AMC ^b | NIH-3T3 | 1 day | | 2 | |
| Jia et al. ⁶² | MAO-CS ^c | MC3T3-E1 | 8 h | | 1, 2, 4 | |

^aMicroarc oxidation. ^bPoly(γ-glutamic acid)-g-7-amino-4-methylcoumarin. ^cChitosan.

- (2) Chen, Y.; Xu, Z.; Smith, C.; Sankar, J. Recent advances on the development of magnesium alloys for biodegradable implants. *Acta Biomater.* **2014**, *10* (11), 4561–4573.
- (3) Zeng, R.; Dietzel, W.; Witte, F.; Hort, N.; Blawert, C. Progress and Challenge for Magnesium Alloys as Biomaterials. *Adv. Eng. Mater.* **2008**, *10* (8), B3–B14.
- (4) Witte, F.; Hort, N.; Vogt, C.; Cohen, S.; Kainer, K. U.; Willumeit, R.; Feyerabend, F. Degradable biomaterials based on magnesium corrosion. *Curr. Opin. Solid State Mater. Sci.* **2008**, 12 (5–6), 63–72.
- (5) Xin, Y.; Hu, T.; Chu, P. K. *In vitro* studies of biomedical magnesium alloys in a simulated physiological environment: a review. *Acta Biomater.* **2011**, *7* (4), 1452–1459.
- (6) Witte, F.; Fischer, J.; Nellesen, J.; Crostack, H. A.; Kaese, V.; Pisch, A.; Beckmann, F.; Windhagen, H. *In vitro* and in vivo corrosion measurements of magnesium alloys. *Biomaterials* **2006**, *27* (7), 1013–1018
- (7) Zhao, D.; Witte, F.; Lu, F.; Wang, J.; Li, J.; Qin, L. Current status on clinical applications of magnesium-based orthopaedic implants: A review from clinical translational perspective. *Biomaterials* **2017**, *112*, 287–302.
- (8) Li, Z.; Gu, X.; Lou, S.; Zheng, Y. The development of binary Mg-Ca alloys for use as biodegradable materials within bone. *Biomaterials* **2008**, 29 (10), 1329–1344.
- (9) Witte, F.; Kaese, V.; Haferkamp, H.; Switzer, E.; Meyer-Lindenberg, A.; Wirth, C. J.; Windhagen, H. In vivo corrosion of four magnesium alloys and the associated bone response. *Biomaterials* **2005**, *26* (17), 3557–3563.
- (10) Hornberger, H.; Virtanen, S.; Boccaccini, A. R. Biomedical coatings on magnesium alloys a review. *Acta Biomater.* **2012**, *8* (7), 2442–2455.
- (11) Wang, J.; Tang, J.; Zhang, P.; Li, Y.; Wang, J.; Lai, Y.; Qin, L. Surface modification of magnesium alloys developed for bioabsorbable orthopedic implants: a general review. *J. Biomed. Mater. Res., Part B* **2012**, *100* (6), 1691–1701.
- (12) Lellouche, J.; Kahana, E.; Elias, S.; Gedanken, A.; Banin, E. Antibiofilm activity of nanosized magnesium fluoride. *Biomaterials* **2009**, *30* (30), 5969–5978.
- (13) Pereda, M. D.; Alonso, C.; Burgos-Asperilla, L.; del Valle, J. A.; Ruano, O. A.; Perez, P.; Fernandez Lorenzo de Mele, M. A. Corrosion inhibition of powder metallurgy Mg by fluoride treatments. *Acta Biomater.* **2010**, *6* (5), 1772–1782.
- (14) Witte, F.; Fischer, J.; Nellesen, J.; Vogt, C.; Vogt, J.; Donath, T.; Beckmann, F. In vivo corrosion and corrosion protection of magnesium alloy LAE442. *Acta Biomater.* **2010**, *6* (5), 1792–1799.
- (15) Kunjukunju, S.; Roy, A.; Ramanathan, M.; Lee, B.; Candiello, J. E.; Kumta, P. N. A layer-by-layer approach to natural polymer-derived bioactive coatings on magnesium alloys. *Acta Biomater.* **2013**, 9 (10), 8690–8703.
- (16) Sun, J.; Liu, X.; Meng, L.; Wei, W.; Zheng, Y. One-step electrodeposition of self-assembled colloidal particles: a novel strategy for biomedical coating. *Langmuir* **2014**, *30* (37), 11002–11010.
- (17) Zomorodian, A.; Garcia, M. P.; Moura e Silva, T.; Fernandes, J. C.; Fernandes, M. H.; Montemor, M. F. Corrosion resistance of a composite polymeric coating applied on biodegradable AZ31 magnesium alloy. *Acta Biomater.* **2013**, *9* (10), 8660–8670.
- (18) Li, N.; Li, Y. D.; Wang, Y. B.; Li, M.; Cheng, Y.; Wu, Y. H.; Zheng, Y. F. Corrosion resistance and cytotoxicity of a MgF₂coating on biomedical Mg-1Ca alloy via vacuum evaporation deposition method. *Surf. Interface Anal.* **2013**, 45 (8), 1217–1222.
- (19) Boudou, T.; Crouzier, T.; Ren, K.; Blin, G.; Picart, C. Multiple functionalities of polyelectrolyte multilayer films: new biomedical applications. *Adv. Mater.* **2010**, 22 (4), 441–67.
- (20) Koh, L.-D.; Cheng, Y.; Teng, C.-P.; Khin, Y.-W.; Loh, X.-J.; Tee, S.-Y.; Low, M.; Ye, E.; Yu, H.-D.; Zhang, Y.-W.; Han, M.-Y. Structures, mechanical properties and applications of silk fibroin materials. *Prog. Polym. Sci.* **2015**, *46*, 86–110.
- (21) Leal-Egaña, A.; Scheibel, T. Silk-based materials for biomedical applications. *Biotechnol. Appl. Biochem.* **2010**, *55* (3), 155–167.

- (22) Thurber, A. E.; Omenetto, F. G.; Kaplan, D. L. In vivo bioresponses to silk proteins. *Biomaterials* **2015**, *71*, 145–157.
- (23) Kundu, B.; Kurland, N. E.; Bano, S.; Patra, C.; Engel, F. B.; Yadavalli, V. K.; Kundu, S. C. Silk proteins for biomedical applications: Bioengineering perspectives. *Prog. Polym. Sci.* **2014**, 39 (2), 251–267.
- (24) You, R.; Xu, Y.; Liu, G.; Liu, Y.; Li, X.; Li, M. Regulating the degradation rate of silk fibroin films through changing the genipin crosslinking degree. *Polym. Degrad. Stab.* **2014**, *109*, 226–232.
- (25) Ruan, Q. X.; Zhou, P.; Hu, B. W.; Ji, D. An investigation into the effect of potassium ions on the folding of silk fibroin studied by generalized two-dimensional NMR-NMR correlation and Raman spectroscopy. *FEBS J.* **2008**, 275 (2), 219–32.
- (26) Borkner, C. B.; Elsner, M. B.; Scheibel, T. Coatings and films made of silk proteins. ACS Appl. Mater. Interfaces 2014, 6 (18), 15611–25.
- (27) Jin, H. J.; Park, J.; Karageorgiou, V.; Kim, U. J.; Valluzzi, R.; Cebe, P.; Kaplan, D. L. Water-Stable Silk Films with Reduced β -Sheet Content. *Adv. Funct. Mater.* **2005**, *15* (8), 1241–1247.
- (28) Kikuchi, M.; Itoh, S.; Ichinose, S.; Shinomiya, K.; Tanaka, J. Self-organization mechanism in a bone-like hydroxyapatite/collagen nanocomposite synthesized *in vitro* and its biological reaction in vivo. *Biomaterials* **2001**, 22 (13), 1705–1711.
- (29) Midha, S.; Murab, S.; Ghosh, S. Osteogenic signaling on silk-based matrices. *Biomaterials* **2016**, *97*, 133–153.
- (30) Gu, Z. P.; Xie, H. X.; Huang, C. C.; Peng, H.; Tan, H.; Li, L.; Yu, X. X. Effects of strontium-doped calcium polyphosphate on angiogenic growth factors expression of co-culturing system *in vitro* and of host cell in vivo. *RSC Adv.* **2014**, *4* (6), 2783–2792.
- (31) Qiu, K.; Zhao, X. J.; Wan, C. X.; Zhao, C. S.; Chen, Y. W. Effect of strontium ions on the growth of ROS17/2.8 cells on porous calcium polyphosphate scaffolds. *Biomaterials* **2006**, *27* (8), 1277–86.
- (32) Han, J.; Wan, P.; Sun, Y.; Liu, Z.; Fan, X.; Tan, L.; Yang, K. Fabrication and Evaluation of a Bioactive Sr—Ca—P Contained Micro-Arc Oxidation Coating on Magnesium Strontium Alloy for Bone Repair Application. J. Mater. Sci. Technol. 2016, 32 (3), 233—
- (33) Du, C.; Jin, J.; Li, Y.; Kong, X.; Wei, K.; Yao, J. Novel silk fibroin/hydroxyapatite composite films: Structure and properties. *Mater. Sci. Eng., C* **2009**, 29 (1), 62–68.
- (34) Ming, J.; Zuo, B. A novel electrospun silk fibroin/hydroxyapatite hybrid nanofibers. *Mater. Chem. Phys.* **2012**, *137* (1), 421–427.
- (35) Lin, F.; Li, Y.; Jin, J.; Cai, Y.; Wei, K.; Yao, J. Deposition behavior and properties of silk fibroin scaffolds soaked in simulated body fluid. *Mater. Chem. Phys.* **2008**, *111* (1), 92–97.
- (36) Wang, L.; Ning, G. L.; Senna, M. Microstructure and gelation behavior of hydroxyapatite-based nanocomposite sol containing chemically modified silk fibroin. *Colloids Surf., A* **2005**, 254 (1–3), 159–164.
- (37) Kong, X. D.; Cui, F. Z.; Wang, X. M.; Zhang, M.; Zhang, W. Silk fibroin regulated mineralization of hydroxyapatite nanocrystals. *J. Cryst. Growth* **2004**, 270 (1–2), 197–202.
- (38) Kim, H. J.; Kim, U. J.; Kim, H. S.; Li, C. M.; Wada, M.; Leisk, G. G.; Kaplan, D. L. Bone tissue engineering with premineralized silk scaffolds. *Bone* **2008**, *42* (6), 1226–1234.
- (39) Bhumiratana, S.; Grayson, W. L.; Castaneda, A.; Rockwood, D. N.; Gil, E. S.; Kaplan, D. L.; Vunjak-Novakovic, G. Nucleation and growth of mineralized bone matrix on silk-hydroxyapatite composite scaffolds. *Biomaterials* **2011**, 32 (11), 2812–2820.
- (40) Rockwood, D. N.; Preda, R. C.; Yucel, T.; Wang, X.; Lovett, M. L.; Kaplan, D. L. Materials fabrication from Bombyx mori silk fibroin. *Nat. Protoc.* **2011**, *6* (10), 1612–1631.
- (41) Dewair, M.; Baur, X.; Ziegler, K. Use of immunoblot technique for detection of human IGE and IGG antibodies to individual silk proteins. *J. Allergy Clin. Immunol.* **1985**, *76* (4), 537–542.
- (42) Wang, X.; Partlow, B.; Liu, J.; Zheng, Z.; Su, B.; Wang, Y.; Kaplan, D. L. Injectable silk-polyethylene glycol hydrogels. *Acta Biomater.* **2015**, *12*, 51–61.

- (43) Pei, Y.; Liu, X.; Liu, S.; Lu, Q.; Liu, J.; Kaplan, D. L.; Zhu, H. A mild process to design silk scaffolds with reduced beta-sheet structure and various topographies at the nanometer scale. *Acta Biomater.* **2015**, 13, 168–76.
- (44) Gotoh, Y.; Tsukada, M.; Baba, T.; Minoura, N. Physical properties and structure of poly(ethylene glycol)-silk fibroin conjugate films. *Polymer* **1997**, 38 (2), 487–490.
- (45) Bakhsheshi-Rad, H. R.; Idris, M. H.; Abdul-Kadir, M. R. Synthesis and *in vitro* degradation evaluation of the nano-HA/MgF₂ and DCPD/MgF₂ composite coating on biodegradable Mg-Ca-Zn alloy. *Surf. Coat. Technol.* **2013**, 222, 79–89.
- (46) Bayraktar, O.; Malay, O.; Ozgarip, Y.; Batigun, A. Silk fibroin as a novel coating material for controlled release of theophylline. *Eur. J. Pharm. Biopharm.* **2005**, *60* (3), 373–381.
- (47) Lu, Q.; Hu, X.; Wang, X.; Kluge, J. A.; Lu, S.; Cebe, P.; Kaplan, D. L. Water-insoluble silk films with silk I structure. *Acta Biomater.* **2010**, *6* (4), 1380–1387.
- (48) Chehimi, M. M.; Delamar, M. X-ray photoelectron spectroscopy of merocyanine dyes: Part VIII. Partial charge and conjugation of heteroatoms in the electroattractor rings. *J. Electron Spectrosc. Relat. Phenom.* 1990, 50 (4), C25–C32.
- (49) Sugama, T.; Kukacka, L.; Carciello, N.; Hocker, N. Study of interactions at water-soluble polymer/Ca (OH)₂ or gibbsite interfaces by XPS. *Cem. Concr. Res.* **1989**, *19* (6), 857–867.
- (50) Di Castro, V.; Polzonetti, G. XPS study of MnO oxidation. J. Electron Spectrosc. Relat. Phenom. 1989, 48 (1), 117–123.
- (51) Liu, J.; Liu, X. L.; Xi, T. F.; Chu, C. C. A novel pseudo-protein-based biodegradable coating for magnesium substrates: *in vitro* corrosion phenomena and cytocompatibility. *J. Mater. Chem. B* **2015**, 3 (5), 878–893.
- (52) Abdal-hay, A.; Barakat, N. A. M.; Lim, J. K. Hydroxyapatite-doped poly(lactic acid) porous film coating for enhanced bioactivity and corrosion behavior of AZ31 Mg alloy for orthopedic applications. *Ceram. Int.* **2013**, 39 (1), 183–195.
- (53) Sun, M.; Yerokhin, A.; Bychkova, M. Y.; Shtansky, D. V.; Levashov, E. A.; Matthews, A. Self-healing plasma electrolytic oxidation coatings doped with benzotriazole loaded halloysite nanotubes on AM50 magnesium alloy. *Corros. Sci.* **2016**, *111*, 753–769.
- (54) Scully, J. R. Polarization resistance method for determination of instantaneous corrosion rates. *Corrosion* **2000**, *56* (2), 199–218.
- (55) Picart, C. Polyelectrolyte multilayer films: From physicochemical properties to the control of cellular processes. *Curr. Med. Chem.* **2008**, *15* (7), 685–697.
- (56) Wang, J.; He, Y.; Maitz, M. F.; Collins, B.; Xiong, K.; Guo, L.; Yun, Y.; Wan, G.; Huang, N. A surface-eroding poly(1,3-trimethylene carbonate) coating for fully biodegradable magnesium-based stent applications: toward better biofunction, biodegradation and biocompatibility. *Acta Biomater.* **2013**, *9* (10), 8678–89.
- (57) Sun, J.; Zhu, Y.; Meng, L.; Wei, W.; Li, Y.; Liu, X.; Zheng, Y. Controlled release and corrosion protection by self-assembled colloidal particles electrodeposited onto magnesium alloys. *J. Mater. Chem. B* **2015**, 3 (8), 1667–1676.
- (58) Yun, Y.; Dong, Z.; Yang, D.; Schulz, M. J.; Shanov, V. N.; Yarmolenko, S.; Xu, Z.; Kumta, P.; Sfeir, C. Biodegradable Mg corrosion and osteoblast cell culture studies. *Mater. Sci. Eng., C* **2009**, 29 (6), 1814–1821.
- (59) McNamara, S. L.; Rnjak-Kovacina, J.; Schmidt, D. F.; Lo, T. J.; Kaplan, D. L. Silk as a biocohesive sacrificial binder in the fabrication of hydroxyapatite load bearing scaffolds. *Biomaterials* **2014**, *35* (25), 6941–6953.
- (60) Peng, S.; Zhou, G.; Luk, K. D.; Cheung, K. M.; Li, Z.; Lam, W. M.; Zhou, Z.; Lu, W. W. Strontium promotes osteogenic differentiation of mesenchymal stem cells through the Ras/MAPK signaling pathway. *Cell. Physiol. Biochem.* **2009**, 23 (1–3), 165–174.
- (61) Gu, X. N.; Li, N.; Zhou, W. R.; Zheng, Y. F.; Zhao, X.; Cai, Q. Z.; Ruan, L. Corrosion resistance and surface biocompatibility of a microarc oxidation coating on a Mg-Ca alloy. *Acta Biomater.* **2011**, 7 (4), 1880–1889.

(62) Jia, Z.; Xiong, P.; Shi, Y.; Zhou, W.; Cheng, Y.; Zheng, Y.; Xi, T.; Wei, S. Inhibitor encapsulated, self-healable and cytocompatible chitosan multilayer coating on biodegradable Mg alloy: a pH-responsive design. *J. Mater. Chem. B* **2016**, *4* (14), 2498–2511.